Majalah Obat Tradisional (Trad. Med. J.), September-December 2024
Vol. 29(3), p 327-343
ISSN-p : 1410-5918 ISSN-e : 2406-9086

Submitted : 20-02-2024
Revised : 02-07-2024
Accepted : 12-09-2024

# Characterization and Antioxidant Potential of *Acacia nilotica* Synthesized Callus and Seed Nanoparticles

**Ifeanyi Jude Ibe[1], Hauwa Ahmed Zailani[1], Mubarak Muhammad Dahiru[2]*, Ishaku Adamu Gali[3]**

[1] Department of Biochemistry, Faculty of Life Sciences, Modibbo Adama University, Yola, Jimeta, Adamawa State, Nigeria

[2] Department of Pharmaceutical Technology, School of Science and Technology, Adamawa State Polytechnic, Yola, Jimeta, Adamawa State, Nigeria

[3] Department of Biotechnology, Faculty of Life Sciences, Modibbo Adama University, Yola, Jimeta, Adamawa State, Nigeria

## ABSTRACT

This research aimed to explore the callogenesis, characterization, and antioxidant potential of *Acacia nilotica* callus and seed silver nanoparticles. The callus induction was accomplished using plant growth hormones. The silver nanoparticles (AgNPs) were synthesized from the seed and callus extracts and characterized using Gas chromatography-mass spectroscopy (GC-MS), X-ray diffraction (XRD), and Scanning electron microscopy (SEM). The antioxidant activities were evaluated by 1, 1-diphenyl-2-picrylhydrazyl (DPPH), ferric reducing antioxidant power (FRAP) assays, molecular docking, and molecular dynamics simulations. The callus formation ranged from 77% to 100%. The AgNPs exhibited a face-centered cubic structure with the size predicted to be 25 nm while the SEM images showed the AgNPs had clustered topography and variable surface morphology. Exactly 33 and 26 compounds were respectively identified in the callus and seed with 8-Hexadecenal 14-methyl- (Z)- (7.71%) and linoleic acid (15.77%) being the most abundant, respectively. A significantly ($p < 0.05$) higher DPPH and FRAP activities were demonstrated by the callus at the highest dose (1 mg/ml). Moreover, 22-Stigmasten-3-one and 3-(azepan-1-yl)-1,2-benzothiazole 1,1-dioxide, respectively from the callus and seed exhibited the most favorable docking interactions with xanthine oxidase, cytochrome P450 21A2, and myeloperoxidase with a possible activity disruption. Conclusively, the callogenesis technique might be regarded as a reliable alternative to produce pharmacologically active secondary metabolites and nanoparticles against oxidative stress-linked ailments. Moreover, 22-Stigmasten-3-one and 3-(azepan-1-yl)-1,2-benzothiazole 1,1-dioxide might be good starting materials for novel therapeutics synthesis against oxidative stress.

**Keywords:** Callus; GC-MS analysis; Oxidative stress; Molecular docking; Molecular dynamics

## INTRODUCTION

Medicinal plants possess numerous bioactive components that may be utilized for developing new drugs and precursors from which these drugs are developed (Atanasov et al., 2021). An important approach to exploring the pharmaceutical potential of plants is through tissue culture-based techniques (Hasnain et al., 2022). Callogenesis simply termed as producing callus tissue from undifferentiated plant cells is an important tool in plant biotechnology and pharmacological research (de Oliveira et al., 2020). The callogenesis technique is important in both basic and industrial settings (Ishaku et al., 2020). *A. nilotica* belongs to the Fabaceae family and is also referred to as the gum Arabic tree, *Bagaruwa* in Hausa (Nigeria), *Odanwoma* in Akan (Ghana), and *Boni* in Ewe (Togo). It is extensively linked with many pharmacological qualities, often used in traditional medicine to treat illnesses such as respiratory infections, skin diseases, and gastrointestinal disorders (Batiha et al., 2022). Callus cultures obtained from different plant parts, including the leaves, stems, roots, and seeds contain secondary metabolites with various pharmacological properties (de Oliveira et al., 2020).

Medicinal plants have been linked to different pharmacological activities, including antioxidant and antidiabetic effects, making them invaluable therapeutic sources (Dahiru & Nadro, 2022a; Dahiru, 2023; Dahiru et al., 2023b). Green AgNPs synthesis *via* plants is becoming popular due to its availability, eco-friendliness, and potential medicinal applications (Rahuman et al., 2022). *A. nilotica* has been reported as a good source for nanoparticle synthesis including AgNPs. The nanoparticles synthesized using these plant extracts exhibit several therapeutic activities, including anticancer, antioxidant, and antimicrobial activities (Ahn & Park, 2020;

***Corresponding author : Mubarak Muhammad Dahiru**
**Email : mubaraq93@adamawastatepoly.edu.ng**

Zubair et al., 2022; Jaison et al., 2023; Mohamad et al., 2023). Concerning callogenesis and green AgNPs synthesis, an increase in research interest has been on the rise in the phytochemistry and antioxidant properties of *A. nilotica* recently (Zubair et al., 2022). Even still, significant studies need to be done to completely understand the mechanism of action of the phytochemicals produced from the callus culture and synthesized *via* green synthesis. Nevertheless, this still remains a gap to be explored.

Oxidative stress arises because of an imbalance between reactive oxygen species (ROS) production and subsequent quenching by the inherent antioxidant system within the cell (Korac et al., 2021). ROS are products of many metabolic pathways and enzymes, including xanthine oxidase (Singh et al., 2023), cytochrome p450 21A2 (Veith & Moorthy, 2018), and myeloperoxidase (Chen et al., 2020). These enzymes were reported previously as antioxidant targets (Dahiru et al., 2024a; Dahiru & Musa, 2024; Musa et al., 2024). In ailments leading to the depletion of the inherent antioxidant system, a redox imbalance is established which further exacerbates these ailments, thus requiring exogenous sources of antioxidants to suppress oxidative stress (Oguntibeju, 2019). Several plants have been previously reported to show some antioxidant potentials by providing the reducing power required to quench the generated ROS and are regarded as novel sources of antioxidant therapeutics (Dahiru & Nadro, 2022b; Oh & Kim, 2022; Afrokh et al., 2023; Dahiru et al., 2023a; Dahiru et al., 2024b). Thus, searching for novel antioxidant therapeutics from plant-based sources remains a target for exploration. This research aimed to explore the characterization and antioxidant potential of *A. nilotica* callus and seed AgNPs to identify potential antioxidant therapeutic candidates.

## MATERIALS AND METHODS

### Materials

### Sample collection

Dried samples of *A. nilotica* seed pods were bought from Girei market, Adamawa State, Nigeria. It was botanically identified by a botanist at the Plant Science Department of Modibbo Adama University, Yola, Nigeria. The pods were broken to recover the seeds.

### Chemicals and reagents

Naphthaleneacetic acid (Toku-E Ltd, Japan), 2,4-dichlorophenoxyacetic acid (RPI International, USA), 6-benzyl amino purine (Adooq Bioscience, USA), Murashige and Skoog (Biotrend, Germany), $AgNO_3$ (Flinn Scientific, USA), 1, 1-diphenyl-2-picrylhydrazyl (TCI Ltd, India), Ascorbic acid (Oxford Lab Fine Chem LLP, India), and FRAP reagent (Bioligand Technologies India Private Ltd, India).

### Methods

### Callus induction

The sterilization of *A. nilotica* seed was done in a laminar flow hood (Biobase, LCB-V1300, China). The seeds were surface-sterilized for 3 minutes using 90% ethanol and washed trice with sterilized double-distilled water, then with a 3.5% sodium hypochlorite supplemented with Tween-20 to remove external contaminants on the seed surface. This was rinsed with sterile double-distilled water (Ishaku et al., 2020).

For the callus formation, 2.5 mg/L of 2,4-dichlorophenoxyacetic acid (2, 4-D), 6-benzyl amino purine (BAP) cytokine (1.0 and 1.5 mg/L) and five doses of auxin 1-naphthaleneacetic acid (1-NAA) (0.5, 1.0, 1.5, 2.0 and 2.5mg/L) were used for the treatments. A control group lacking the above-mentioned regulators was used. The Murashige and Skoog basal medium (MS basal media) was supplemented with the regulators, followed by adjusting the pH to 5.8 and supplementation with 0.375 g of phytagels as a solidifying agent. Moreover, the media was sterilized in an autoclave (Allenger**s,** AA-VE23, India**)** at 121°C, 15 psi for 15 minutes, and dispensed into inoculation bottles (Ishaku et al., 2020). The callus proliferation and growth were observed weekly for eight weeks after inoculation in triplicates. They were kept in a growth chamber (Percival Scientific, CU 36L4, USA) at 20°C with 12 hours of photoperiod of light and darkness. The percentage callus induction was determined according to Equation 1.

$$\text{Callus induction} = \frac{\text{Number of explants with response}}{\text{Number of explants inoculated}} \times 100 \quad \text{Equation 1}$$

### Callus and Seed Extract Preparation

The callus was collected, oven-dried at 40˚C, and ground into powder using mortar and pestle, followed by wrapping in aluminum foil for storage at room temperature till further use. The dried seeds were blended into a fine powder, followed by aqueous extraction. Exactly 400 g of the dried seed powder was macerated in 1 L of distilled water for 48 hours, followed by filtration with Whatman filter paper. The filtrate was dried over a water bath at 40°C. The obtained extract was stored at 4˚C till further use.

**AgNPs Preparation and Characterization**

Exactly 10 g of the callus and seed extracts were separately transferred to a 250 ml conical flask, followed by adding 100 ml of sterile double-distilled water and then 30 minutes of heating at 80°C. These were filtered after cooling and the filtrates (10 ml) were separately mixed with 90 ml of 1 mM $AgNO_3$, followed by 48 hours of 35°C incubation in the dark. The color changes were recorded and the AgNPs were collected by 15 minutes of centrifugation at 10,000 rpm and dried at 40°C.

The silver ions were reduced and monitored *via* UV-Vis spectrum measurement of the reaction medium, following distilled water dilution of a small aliquot of the sample. A UV-vis spectrophotometer (Shimadzu, UV-1800, USA) was used for spectral analysis at 200–800 nm. XRD characterization was carried out using a Cu-K*α* radiation source in the scattering range of 20-80 on the instrument, operating at a voltage of 45 kV and a current of 40 mA. The morphology and size of the AgNPs were analyzed using SEM (JEOL, JEM-1400, Japan) by dispersing the sample on a copper grid and drying at room temperature for scanning using SEM. Additionally, the AgNPs size was evaluated using the Debye–Scherrer formula (Equation 2).

$$D = \frac{k\lambda}{\beta\cos\theta} \qquad \text{Equation 2}$$

Where D = particle size (nm), K = 0.9 (a constant), λ = 0.1541 nm (X-ray source wavelength), β = full width at half maximum (FWHM), and θ = Braggs angle.

**GC–MS Analysis**

A combined GC-MS (Agilent 19091-433HP, USA) fused with a silica column was used for compound identification. The procedures and instrumentation settings were as described previously (Dahiru et al., 2022).

**Antioxidant Activity**

**DPPH Method**

The antioxidant potential was determined using the DPPH assay method adopted from Sumazian et al. (2010). The initial DPPH solution absorbance measured without a sample at 517 nm was regarded as a control. Exactly 0.2 ml of varying concentrations (0.2-1.0 mg/ml) of the samples and ascorbic acid (AA) were mixed with 3 ml of 0.1 mM DPPH solution, followed by 30 minutes of incubation in the dark. A UV-visible spectrophotometer (Scitek, SP-UV5100, China) was used to measure the absorbance at 517 nm. The DPPH scavenging activity was calculated according to Equation 3.

$$\%\ \text{DPPH scavenging} = \frac{Ac-As}{Ac} \times 100 \qquad \text{Equation 3}$$

Where Ac and As are the absorbance of the control and sample, respectively.

**FRAP**

The method of Benzie & Strain (1996) was adopted to determine the FRAP of the samples. Briefly, 0.2 ml of varying concentrations (0.2-1.0 mg/ml) of the samples and AA were added to 3.8 ml of the FRAP reagent [10 ml of 0.3 M sodium acetate buffer pH 3.6, 1 ml of 10 mM TPTZ (2,4,6-Tripyridyl- S-Triazine) solution in 40 mM HCL and 1 ml of 20 mM $FeCl_3$ solution], followed by 30 minutes of incubation at 37°C. The absorbance was measured at 593 nm. A solution of the reagents without the samples was used as a control. The antioxidant capacity was expressed according to Equation 4. The result was expressed as the mean of triplicate determinations.

$$\text{FRAP \% Inhibiton} = \frac{Ac-As}{Ac} \times 100 \qquad \text{Equation 4}$$

Where Ac and As are the absorbance of the control and sample, respectively.

***In silico* Antioxidant Activity**

**Ligand and Target Preparation**

The compounds (ligands) identified in the callus and seed of *A. nilotica* were downloaded from the PubChem database in structure data format (SDF) and subjected to Lipinski's rule screening using the DruLiTo software. Only ligands that passed Lipinski's rule of five were selected for the docking. Exactly 8 and 10 compounds from the callus and seed, respectively were non-violators of Lipinski's rule. The ligands were energy-minimized by the Open Babel interface of the PyRx software (version 0.8). The docking targets were downloaded from the RSCB protein data bank database in protein data bank format (PDB). They were prepared using AutodockTools software (version 1.5.7) (Sanner, 1999) by removing all identical additional chains, heteroatoms, water molecules, and ligands, followed by the repair of missing atoms and the addition of polar hydrogens. The ligands from *A. nilotica* callus and seed are shown in Table I, depicting their designation and PubChem IDs while the docking targets are shown in Table II, revealing the docking coordinates (grid box).

**Table I. List of the Ligands from *A. nilotica* Callus and Seed**

| Ligands | | Designation | PubChem ID |
|---|---|---|---|
| Callus | 3-Cyclohexene-1-carboxaldehyde, 4-methyl | I | 111012 |
| | 5-amino-1H-pyrazole-3-carboxamide | II | 50896559 |
| | 3-(azepan-1-yl)-1,2-benzothiazole 1,1-dioxide | III | 535203 |
| | Thunbergol | IV | 5363523 |
| | (*2E*)-Penta-2,4-dienoic acid | V | 642034 |
| | 22-Stigmasten-3-one | VI | 91692436 |
| | Isobutyraldehyde allylhydrazone | VII | 5362617 |
| | Ethyl-spiro-2-3-hexane-1-carboxylate | VIII | 533443 |
| Seed | Methionol | IX | 10448 |
| | 2,2-dimethyl-cyclopentane-1,3-dione | X | 19763 |
| | 5-Hydroxymethylfurfural | XI | 237332 |
| | 4-Mercaptophenol | XII | 240147 |
| | 5-Amino-2H-pyrazole-3-carboxamide | XIII | 50896559 |
| | 3-(azepan-1-yl)-1,2-benzothiazole 1,1-dioxide | XIV | 535203 |
| | 2-(3-Hydroxybutyl) cyclooctanone | XV | 543346 |
| | Benzo[c]thiophene-1-carboxylic acid, 4,5,6,7-tetrahydro-, (2-dimethylaminoethyl) amide | XVI | 719165 |
| | Melamine | XVII | 7955 |
| | Carbonic acid, propargyl 2,2,2-trichloroethyl ester | XVIII | 91691208 |

**Table II. Docking Targets and Respective Coordinates**

| Target | Docking Coordinates | | |
|---|---|---|---|
| | X | Y | Z |
| Xanthine oxidase (XO) | 23.48 | -16.11 | 35.99 |
| Cytochrome P450 21A2 (CytP450 21A2) | -14.76 | 11.82 | 28.55 |
| Myeloperoxidase (MPO) | 19.52 | -13.60 | -4.52 |

**MD and MDS**

The docking pockets were identified using the Pranweb; Ligand Binding Site Prediction online server (Jendele et al., 2019), revealing the pockets with the highest ligand docking probability on the target surface. MD was done using the Vina Wizard of the PyRx software to determine the top docked compound with the lowest binding affinity (BA) whereas Equation 5 was used to determine the inhibition constant (Ki) from the BA (Ortiz et al., 2019). The docked complex visualization was done with Discovery Studio visualizer (version 16.1.0) to reveal the dock pose and interactions. Moreover, only the top-docked compounds with the lowest BA and Ki were presented and further subjected to MDS. The MDS of the undocked and ligand-docked target was done using the CABflex server V2.0 online server (Kurcinski et al., 2019) to determine the root-mean-square fluctuations (RMSF) of residues of the complex.

$$Ki = \exp \frac{\Delta G}{RT} \qquad \text{Equation 5}$$

Where; T=298.15 K (temperature); R=1.985 x $10^{-3}$ $kcal^{-1}$ $mol^{-1}$ $k^{-1}$ (the universal gas constant); ΔG = BA

**Statistical Analysis**

The obtained data was expressed as mean ± standard error of the mean (± SEM) and analyzed by one-way analysis of variance and Tukey's multiple comparison tests at $p < 0.05$ level of significance. The Statistical Package for Social Sciences (SPSS) version 22 software was used for the statistical analysis.

## RESULTS

**Callus induction**

Table III shows the callus induction result with different treatments. Treatment 1 had the lowest (77%) callus formation while Treatment 3 and 4 had the highest (100%). Furthermore, there were no morphogenic responses on the medium-cultured cotyledons lacking growth regulators (T0) after eight weeks.

**Characterization of the *A. nilotica* Callus and Seed AgNPs**

Figures 1a and 1b show the XRD spectrum of AgNPs of *A. nilotica* callus and seed, respectively. The result of the XRD pattern of both the callus and seed shows major diffraction peaks at 38.04°,

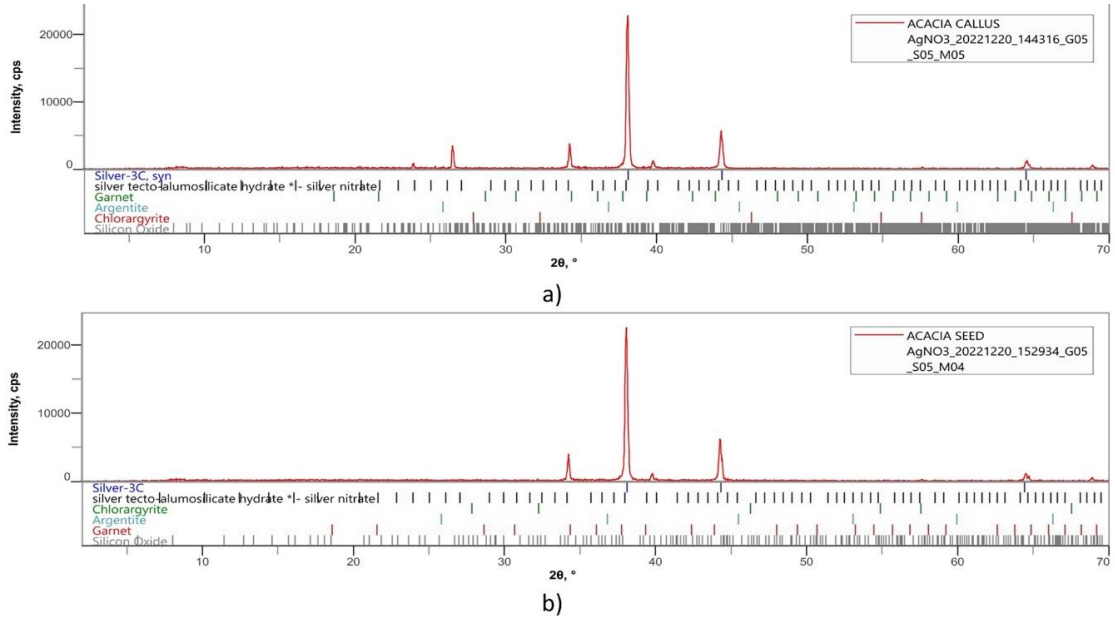


**Figure 1. X-ray Diffraction Spectrum of *A. nilotica* AgNPs; a) Callus and b) Seed. The various peaks shown indicate the intensity of the diffractions at 2θ° and the formation of AgNPs.**

**Table III. Callus Induction**

| Treatment | Concentration of plant growth hormone (mg/L) | Callus induction (%) | Color and Texture |
|---|---|---|---|
| **T0** | 0.0 BAP + 0.0 2,4-D + 0.0 NAA | 0 ±0.00 | Nil |
| **T1** | 0.5 BAP + 1.0 2,4-D + 0.5 NAA | 77 ±1.01 | Brown, Friable |
| **T2** | 0.5 BAP + 1.0 2,4-D + 1.0 NAA | 88 ±0.89 | Brown, Friable |
| **T3** | 0.5 BAP + 1.0 2,4-D + 1.5 NAA | 100 ±0.00 | Brown, Friable |
| **T4** | 0.5 BAP + 1.0 2,4-D + 2.0 NAA | 100 ±0.00 | Brown, Friable |

Values are means ± SEM of three replicates

44.23°, and 64.50° of 2θ respectively corresponding to the (111), (200), and (220) Bragg's reflections of the face-centered cubic structure of silver. The highest peak (38.04°) which corresponds to the (111) lattice plane indicated the preferred orientation of the cubic structure with the AgNPs size predicted to be 25 nm, determined from the Debye-Scherrer Equation.

Figure 2 shows the SEM micrographs of AgNPs of *A. nilotica* callus and seed. The SEM micrographs showed clustered topography and variable surface morphology in terms of shape and size. However, some of the AgNPs were observed to agglomerate in some portions.

**GC-MS analysis**

The compounds identified in the callus of *A. nilotica* are presented in Table IV, revealing the retention time (RT), area, molecular weight (MW), and molecular formula (MF). Exactly 33 compounds were identified with 8-Hexadecenal, 14-methyl-, (Z)- (7.71%), 2-Hydroxycyclopentadecanone (7.25%), and 1-methyl-4-(prop-1-en-2-yl)-3-(3,7,11,15 tetra methyl-hexadeca-1,10E-dien-7-yl)-cyclohex-1-ene (6.36%) being the most abundant. Moreover, most of the compounds were fatty acids while others included ketones, aldehydes, pyrazoles, and thiazoles. Additionally, the structures of the major compounds identified compounds in the *A. nilotica* callus are presented in Figure 3.

Table V shows the RT, percentage area, MW, and MF of the identified compounds in the *A. nilotica* seed. Exactly 26 compounds were identified with linoleic acid (15.77%), palmitic acid (15.26%), and linoelaidic acid (12.1%) being the most abundant. Moreover, the structures of the major compounds identified in the seed extract of *A. nilotica* are presented in Figure 4.

**Antioxidant Activity**

**DPPH**

The DPPH radical scavenging activity of *A. nilotica* callus and seed is exhibited in Figure 5a. The result showed a dose-dependently increased antioxidant activity of the callus and seed. The

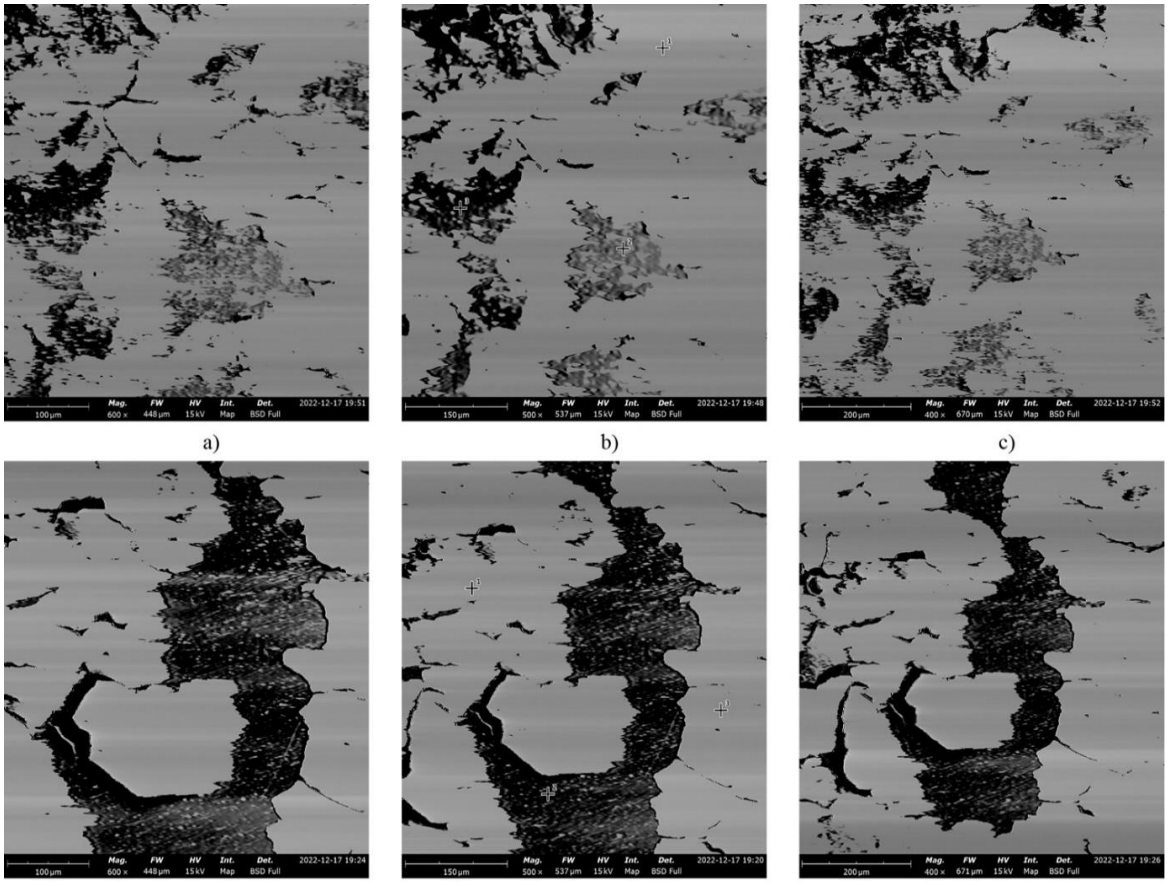


**Figure 2. SEM images of AN AgNPs at 100 µm, 150 µm, and 200 µm, respectively; callus (a, b, c) and seed (d, e, f). The irregular shape of clustered topography of the AgNPs can be observed from the SEM image, depicting different sizes and shapes due to agglomeration of biomolecules by the silver ligand.**

callus exhibited a significantly higher ($p < 0.05$) inhibition (41.84% ±0.98 and 81.87% ±0.20) than the seed (33.82% ±0.98 and 70.82% ±0.50) at 0.2 and 1.0 mg/ml, respectively. Additionally, the callus and seed demonstrated significantly ($p < 0.05$) lower scavenging DPPH activity than AA. Moreover, both the callus (0.41 mg/ml ±0.02) and seed (0.56 mg/ml ±0.01) exhibited significantly higher ($p < 0.05$) $IC_{50}$ than AA (0.20 mg/ml ±0.01).

**FRAP**

The FRAP of *A. nilotica* callus and seed is presented in Figure 5b. The FRAP showed a concentration-dependent upregulated activity, similar to the DPPH method. The callus exhibited a significantly ($p < 0.05$) higher (77.67% ±0.38) inhibition than the seed (65.82% ±0.47) at 1.0 mg/ml though both were significantly lower than AA (91.40% ±0.40). Furthermore, the callus demonstrated a significantly ($p < 0.05$) lower (0.51 mg/ml ±0.02) $IC_{50}$ than the seed (0.70 mg/ml ±0.01) though both were significantly ($p < 0.05$) higher than AA (0.40 mg/ml ±0.02).

***In silico* Antioxidant Activity**

**MD and MDS**

The docking interactions of XO, CytP450 21A2, and MPO with compounds VI and XIV, respectively identified from the *A. nilotica* callus and seed are shown in Table VI. Compound VI was the top docked compound from the callus with all the targets, yielding the lowest BA and Ki. Notable alkyl interactions were observed between VI and XO with BA and Ki of -9.5 kcal/mol and 0.11 µM, respectively. Although both CytP450 21A2 and MPO had the same BA (-9.9 kcal/mol) and Ki (0.05 µM) interacting with VI, a hydrogen bond (HB) interaction with Phe147 in MPO was absent in CytP450 21A2. The lowest BA and Ki were exhibited by compound XIV for the seed extract, thus the top docked compound with all the targets. The lowest BA (-8.6 kcal/mol) and Ki (0.49 µM) were exhibited by the interaction of XIV with XO, inclusive of hydrogen and alkyl interactions. The least favorable interaction of XIV was with MPO with the highest BA and Ki of -7.3 kcal/mol and

**Table IV. Identified Compounds in the AN Callus**

| S/N | Compound Name | RT | Area (%) | MF | MW |
|---|---|---|---|---|---|
| 1 | Trans-3,4-Epoxynonane | 5.78 | 0.52 | $C_9H_{18}O$ | 142.24 |
| 2 | Isobutyraldehyde allylhydrazone | 6.54 | 1.07 | $C_7H_{14}N_2$ | 126.2 |
| 3 | 5-Amino-2H-pyrazole-3-carboxamide | 6.69 | 0.16 | $C_4H_6N_4O$ | 126.12 |
| 4 | (*2E*)-Penta-2,4-dienoic acid | 6.84 | 0.34 | $C_5H_6O_2$ | 98.1 |
| 5 | Ethyl spiro[2.3]hexane-1-carboxylate | 7.23 | 0.19 | $C_9H_{14}O_2$ | 154.21 |
| 6 | Oleic acid | 7.40 | 0.27 | $C_{18}H_{34}O_2$ | 282.5 |
| 7 | *E*-10-Dodecen-1-ol propionate | 8.21 | 2.69 | $C_{15}H_{28}O_2$ | 240.38 |
| 8 | Melezitose | 8.63 | 1.48 | $C_{18}H_{32}O_{16}$ | 504.4 |
| 9 | cis-11-Hexadecenal | 8.77 | 0.76 | $C_{16}H_{30}O$ | 238.41 |
| 10 | Methyl palmitate | 9.29 | 5.77 | $C_{17}H_{34}O_2$ | 270.5 |
| 11 | Trimethylsilyl 14-acetoxy-3,6,9,12-tetraoxatetradecan-1-oate | 9.63 | 4.56 | $C_{15}H_{30}O_8Si$ | 366.48 |
| 12 | Cellobiose | 9.78 | 1.31 | $C_{12}H_{22}O_{11}$ | 342.3 |
| 13 | Undecanoic acid | 9.99 | 3.28 | $C_{11}H_{22}O_2$ | 186.29 |
| 14 | Methyl oleate | 10.16 | 4.94 | $C_{19}H_{36}O_2$ | 296.5 |
| 15 | Methyl 12-methyltetradecanoate | 10.27 | 2.68 | $C_{16}H_{32}O_2$ | 256.42 |
| 16 | Methyl vaccenate | 10.45 | 2.09 | $C_{19}H_{36}O_2$ | 296.5 |
| 17 | 7,11-Hexadecadienal | 10.59 | 2.64 | $C_{19}H_{36}O_2$ | 296.5 |
| 18 | 2-Hydroxycyclopentadecanone | 10.88 | 7.25 | $C_{15}H_{28}O_2$ | 240.38 |
| 19 | 2-Methyl-Z, Z-3,13-octadecadienol | 11.03 | 3.78 | $C_{19}H_{36}O$ | 280.5 |
| 20 | 13-Octadecenal, (Z)- | 11.22 | 3.72 | $C_{18}H_{34}O$ | 266.5 |
| 21 | 8-Hexadecenal, 14-methyl-, (Z)- | 11.38 | 7.71 | $C_{17}H_{32}O$ | 252.4 |
| 22 | 3-(azepan-1-yl)-1,2-benzothiazole 1,1-dioxide | 11.80 | 1.93 | $C_{13}H_{16}N_2O_2S$ | 264.35 |
| 23 | Linoleic acid | 11.93 | 2.96 | $C_{18}H_{32}O_2$ | 280.4 |
| 24 | Z-8-Methyl-9-tetradecenoic acid | 12.18 | 5 | $C_{15}H_{28}O_2$ | 240.38 |
| 25 | 2-Dodecen-1-yl(-)succinic anhydride | 12.82 | 2.51 | $C_{16}H_{26}O_3$ | 266.38 |
| 26 | 7-Pentadecyne | 13.58 | 2.57 | $C_{15}H_{28}$ | 208.38 |
| 27 | Geranylgeranyl acetate | 14.01 | 2.9 | $C_{22}H_{36}O_2$ | 332.5 |
| 28 | 22-Stigmasten-3-one | 14.30 | 0.68 | $C_{29}H_{48}O$ | 412.7 |
| 29 | 2-Methyl-Z,Z-3,13-octadecadienol | 14.39 | 0.85 | $C_{19}H_{36}O$ | 280.5 |
| 30 | 12-Methyl-E,E-2,13-octadecadien-1-ol | 14.45 | 2.91 | $C_{19}H_{36}O$ | 280.5 |
| 31 | 3-Cyclohexene-1-carboxaldehyde, 4-methyl | 14.82 | 6.36 | $C_8H_{12}O$ | 124.2 |
| 32 | Thunbergol | 16.56 | 1.17 | $C_{20}H_{34}O$ | 290.5 |
| 33 | 1,14-Docosanediol | 17.30 | 0.25 | $C_{22}H_{46}O_2$ | 342.6 |

4.40 µM, respectively, and the absence of alkyl interactions. CytP450 21A2 had an attractive charge interaction in addition to the HB and alkyl interactions found in XO and MPO, similarly depicting a Trp202 alkyl interaction with XO.

The dock poses of compounds VI with XO, CytP45021A2, and MPO are shown in Figure 6, depicting the interacting amino acids. Alkyl interaction was identified as the major type of interaction involved with all the targets. Figure 6 further depicts the docking interactions of XIV with XO, CytP450 21A2, and MPO, revealing the amino acids involved. HB was identified as the major type of interaction in all the targets though there were few and two furthermore attractive charges for CytP450 21A2.

The MDS of the undocked (apo) and docked target is presented in Figure 7, revealing the various RMSFs of the residues and depicting the regions of flexibility (hinges). All the targets show several flexible regions with some having higher RMSF than others. Notable changes in the XO docked complex include the decreased displacement of residues Leu397 (1.68 Å) and 1070 (2.83 Å) with increases at 641 (2.91Å) and 1218 (4.18 Å). Docking of VI to CytP450 21A2 led to increased displacements of residues Leu36 (2.44 Å), Arg133 (2.83 Å), Pro155 (2.80 Å) Ala251 (3.01 Å), Arg426 (3.19 Å) and Gly414 (3.97 Å) while residues Phe215 (2.27 Å), Ala266 (1.85 Å), and Thr369 (1.66 Å) were decreased. MDS of compound VI-MPO docked complex showed increased displacements of residues Cys1 (5.47 Å), Ser227 (3.61 Å), Gly155 (2.61 Å), and Lys488 (3.01 Å) with a decrease at Asp39 (1.02 Å), Val113 (0.18 Å), and Ser565 (0.78 Å).

The MDS of compound XIV docked XO, CytP450 21A2, and MPO is presented in Figure 8,

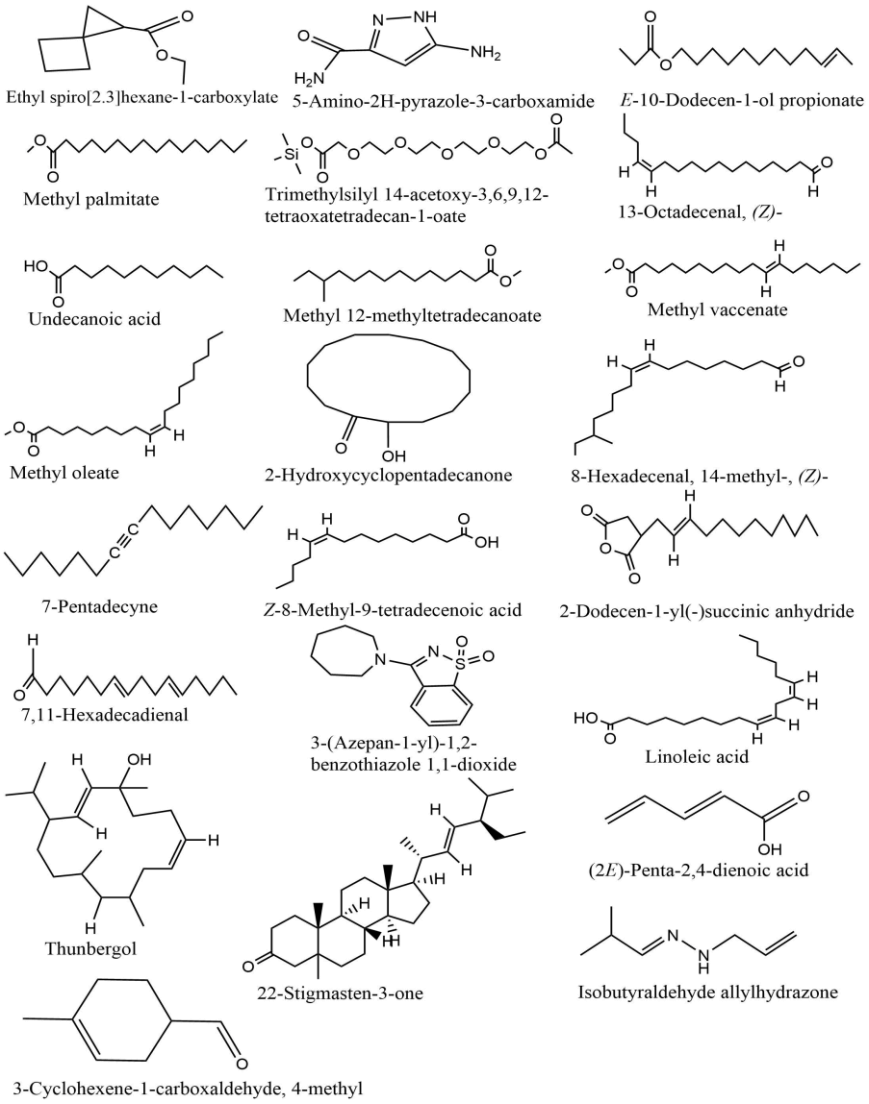


**Figure 3. Structures of the major compounds identified in the *A. nilotica* callus**

exhibiting the RMSF of the apo and docked targets. Residues Thr2 (3.85 Å), Gly502 (3.80 Å), Asp571 (3.64 Å), and Cys1325 (7.70 Å) showed increased displacement in XO whereas Pro224 (2.18 Å), Gly399 (3.05 Å), Pro1012 (1.36 Å), and His1171 (0.614) decreased. For CytP450 21A2, increased displacements were observed for residues Lys29 (3.92 Å), Gly131 (2.67 Å), Gln253 (2.36 Å), Gln276 (3.83 Å) Trp399 (3.06), and Ala426 (3.02) and a decrease at Arg370 (1.38 Å). Several displaced residues were observed for the MPO docked complex with a notable increase at residues Cys1 (5.57 Å), Thr77 (3.16 Å), Gly155 (2.62 Å), Ala104 (5.17 Å), Asp218 (3.55 Å), Pro355 (3.70 Å) and Gly375 (2.37 Å). Additionally, there was a decrease at Gly50 (1.38 Å), Asn139 (3.29 Å), Tyr316 (1.31 Å), Pro471 (1.28 Å), Asn550 (1.18 Å), and Ala578 (2.35 Å).

## DISCUSSION

Auxins and cytokinins are natural plant hormones responsible for plant growth and development. In our study, they were responsible for producing callus from *A. nilotica* seed cotyledon. The callus formation frequency was high, ranging from 77% to 100% on inoculated explant (Table 1). These results agree with the report of Sharma (2017) and Sen et al. (2014), stating that a combined 2, 4-D with BAP and NAA gives higher callus formation. The observed color change from light-yellow to reddish-brown during the reduction process indicates the formation of the AgNPs within the 24 hours stated earlier. This is concurrent with earlier studies confirming AgNPs formation in 24 hours without observing further color change (Lalitha et al., 2013; Namratha & Monica, 2013; Jemal et al., 2017). Additionally,

**Table V. Identified Compounds in the *A. nilotica* Seed**

| S/N | Compound Name | RT | Area % | MF | MW |
|---|---|---|---|---|---|
| 1 | 2,2-dimethyl-cyclopentane-1,3-dione | 4.793 | 0.23 | $C_7H_{10}O_2$ | 126.15 |
| 2 | Melamine | 5.16 | 0.09 | $C_3H_6N_6$ | 126.12 |
| 3 | Methionol | 5.764 | 0.01 | $C_4H_{10}OS$ | 106.19 |
| 4 | 5-Hydroxymethylfurfural | 6.164 | 0.64 | $C_6H_6O_3$ | 126.11 |
| 5 | 4-Mercaptophenol | 6.741 | 0.09 | $C_6H_6OS$ | 126.18 |
| 6 | 5-Amino-2H-pyrazole-3-carboxamide | 6.843 | 0.18 | $C_4H_6N_4O$ | 126.12 |
| 7 | Z, E-2,13-Octadecadien-1-ol | 8.608 | 5.81 | $C_{18}H_{34}O$ | 266.5 |
| 8 | 2-Monoolein | 8.764 | 1.6 | $C_{21}H_{40}O_4$ | 356.5 |
| 9 | Methyl palmitate | 9.28 | 5.47 | $C_{17}H_{34}O_2$ | 270 |
| 10 | Palmitic acid | 9.803 | 15.26 | $C_{16}H_{32}O_2$ | 256 |
| 11 | Methyl oleate | 10.149 | 5.04 | $C_{19}H_{36}O_2$ | 296.5 |
| 12 | Methyl 4,6-dimethyloctanoate | 10.265 | 3.38 | $C_{11}H_{22}O_2$ | 186.29 |
| 13 | 2-Octadecoxyethanol | 10.441 | 2.69 | $C_{20}H_{42}O_2$ | 314.5 |
| 14 | Linoleic acid | 10.624 | 15.77 | $C_{18}H_{32}O_2$ | 280.4 |
| 15 | Linoelaidic acid | 11.025 | 12.1 | $C_{18}H_{32}O_3$ | 280.4 |
| 16 | Linoleoyl chloride | 11.663 | 1.49 | $C_{18}H_{31}ClO$ | 298.9 |
| 17 | Benzo[c]thiophene-1-carboxylic acid, 4,5,6,7-tetrahydro-, (2-dimethylaminoethyl) amide | 11.799 | 4.25 | $C_{13}H_{20}N_2OS$ | 252.38 |
| 18 | 2-octyl-cyclopropaneoctanal | 12.179 | 1.86 | $C_{19}H_{36}O$ | 280.5 |
| 19 | 3-(azepan-1-yl)-1,2-benzothiazole 1,1-dioxide | 13.116 | 1.66 | $C_{13}H_{16}N_2O_2S$ | 264.35 |
| 20 | Cyclopentadecanone, 2-hydroxy- | 13.557 | 7.13 | $C_{15}H_{28}O_2$ | 240.38 |
| 21 | 7-Pentadecyne | 14.732 | 0.19 | $C_{15}H_{28}$ | 208.38 |
| 22 | 2-Linoleoylglycerol | 16.137 | 0.16 | $C_{21}H_{38}O_4$ | 354.5 |
| 23 | Oleic acid | 16.286 | 0.06 | $C_{18}H_{34}O_2$ | 282.5 |
| 24 | Carbonic acid, propargyl 2,2,2-trichloroethyl ester | 16.551 | 0.7 | $C_6H_5Cl_3O_3$ | 231.5 |
| 25 | 2-(3-Hydroxybutyl) cyclooctanone | 17.447 | 0.48 | $C_{12}H_{22}O_2$ | 198.3 |
| 26 | Silane, trimethyl(6-methyl-5-hepten-1-ynyl)- | 17.847 | 0.34 | $C_{11}H_{20}Si$ | 180.36 |

no color change was observed for the control reaction, thus further confirming AgNPs formation. Moreover, the color change might be due to the Surface Plasmon Resonance phenomenon in AgNPs, resulting from the excitation of free electrons (Veerasamy et al., 2011; Roy, 2012). Our study agrees with previous studies on the AgNPs synthesis (Lalitha et al., 2013; Namratha & Monica, 2013; Jemal et al., 2017).

The XRD result revealed the predominantly face-centric cubic nature of the AgNPs, depicted by the diffraction peaks (Figure 1). By file No. 89-8104 of the Joint Committee on Power Diffraction Standards (JCPDS), these obtained peaks could be indexed to the face centric cubic structure. The crystallization of biomolecules from the extracts on the Ag surface might be responsible for the depicted unassigned peaks (Khan et al., 2020; Obidah et al., 2022). Furthermore, previous studies reported similar results for AgNPs synthesis from different plant extracts (Jemal et al., 2017; Khan et al., 2020; Obidah et al., 2022). The properties of the nanoparticles, including surface morphology, size, and shape were determined using SEM. Topographically viewing the SEM micrograph of the AgNPs of the *A. nilotica* callus and seed revealed clustered particles with variation in shape and sizes which might be due to agglomeration of the particles. Additionally, the agglomeration might be due to bio-organic compounds coating the nanoparticles (Khan et al., 2020). Similar results were previously reported (Jemal et al., 2017; Khan et al., 2020; Obidah et al., 2022).

Several compounds (33 and 26) were identified in *A. nilotica* callus and seed, respectively as presented in Tables 4 and 5. Generally, the reliability of medicinal plants for their usage can evaluated by correlating the phytochemical compounds with their biological activities. These compounds exert different pharmacological activities. The antimicrobial, antioxidant, and anti-inflammatory activities of 9,12-octadecadienoic acid *(Z, Z)* have been previously reported (Mathur et al., 2011). Methyl palmitate has been previously associated with antioxidant, anti-inflammatory, and cancer-preventive activities (Arab et al., 2019; Hamed et al., 2020; AbdelJaleel et al., 2021). Arab et al. (2019) reported the modulation of the mitogen-activated protein kinases, nuclear factor, and phosphoinositide 3 kinase/protein kinase B pathways as part of the anti-inflammatory and antioxidant activity of methyl palmitate. In another

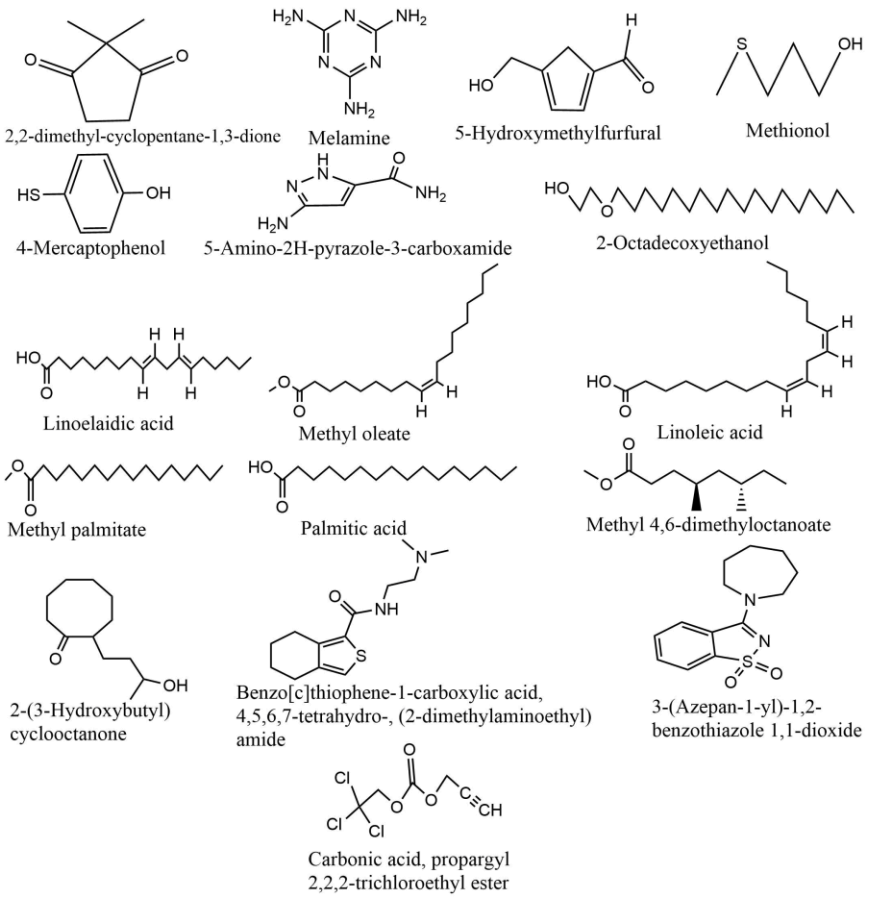


**Figure 4. Structures of the major compounds identified in the *A. nilotica* seed**

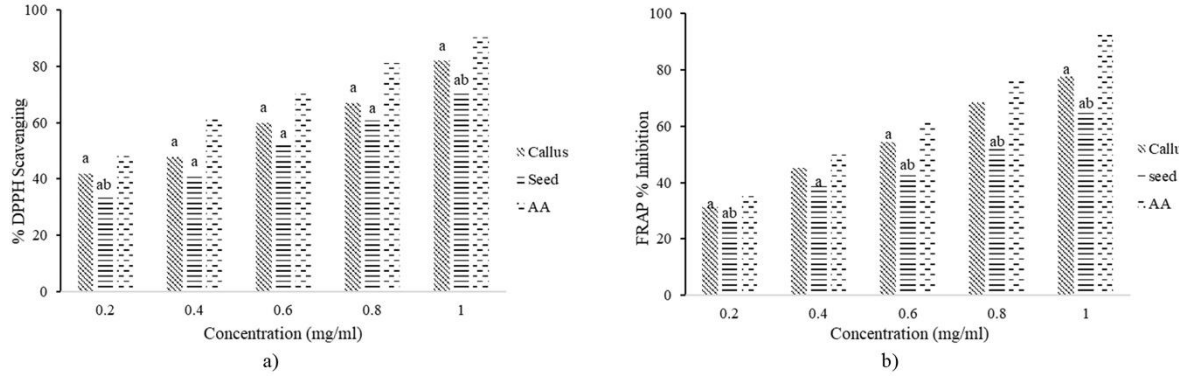


**Figure 5. Antioxidant activity of *A. nilotica* callus and seed by; a) DPPH and b) FRAP methods. Values with a and b denote significantly lower ($p < 0.05$) values than AA and callus, respectively.**

study, AbdelJaleel et al. (2021) reported the inhibition of synovial CD68 macrophages as the anti-inflammatory mechanism of action of methyl palmitate, validating its anti-inflammatory activity. Methyl palmitate ameliorated oxidative stress and inflammatory markers with potential cardioprotective effects and vasodilation activities (Hamed et al., 2020). Thus, this compound might be a significant contributor to *A. nilotica* antioxidant activity reported in our study.

Oxidative stress is vital in the pathology and progression of many diseases, including diabetes and cardiovascular diseases, thus targeting this culprit might alleviate symptoms and bring about relief. In the present study, the potential application of *A. nilotica* in oxidative stress therapy was tested. A dose-dependent increase in the radical scavenging potential of *A. nilotica* was observed for the callus and seed though both were significantly ($P < 0.05$) lower than AA. This might

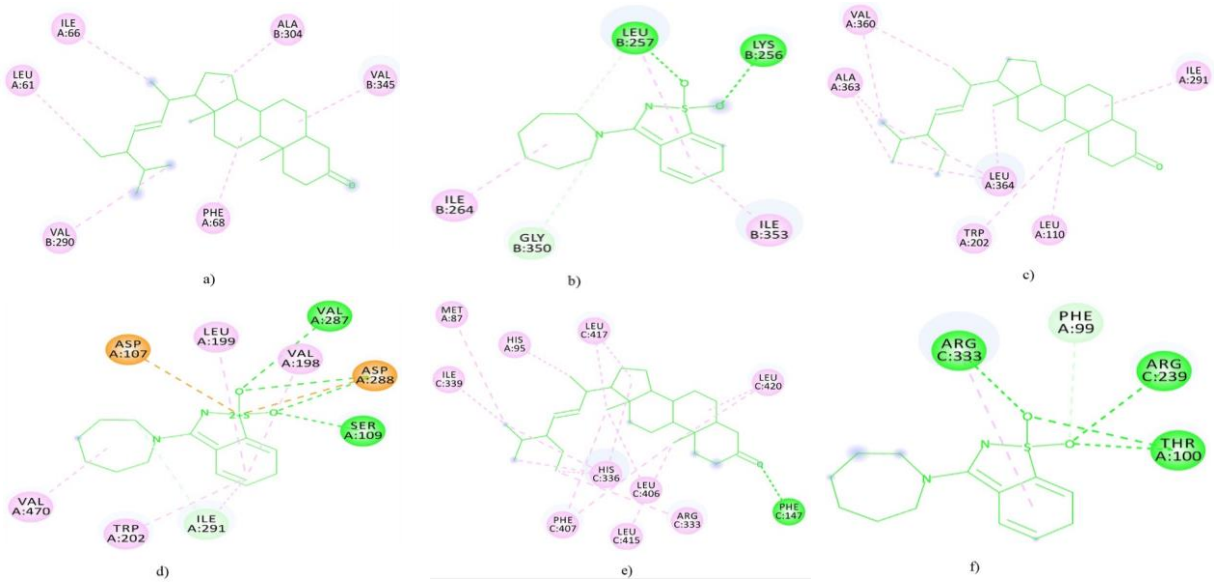


**Figure 6. Docking Interactions of the Targets with Compounds VI and XIV, respectively; XO (a and b), Cytp450 21A2 (c and d), and MPO (e and f). The compounds are centered within the interactions, depicted by their structure, and surrounded by the interacting amino acids. The color of the amino acids indicates the type of interaction with green, pink, and orange colors depicting HB, alkyl, and attractive charge interactions, respectively.**

**Table VI. Docking Interactions of Identified Compounds in the *A. nilotica* Callus and Seed**

| Plant Part | Target | Ligand | BA (kcal/mol) | Ki (µM) | Interaction | Interacting Amino Acid |
|---|---|---|---|---|---|---|
| Callus | XO | VI | -9.5 | 0.11 | Alkyl | Ile66, Leu61, Phe68, Val290, Ala304, Val345 |
| | CytP450 21A2 | VI | -9.9 | 0.05 | Alkyl | Val360, Ala363, Ile291, Trp202, Leu110, 364 |
| | MPO | VI | -9.9 | 0.05 | Hydrogen bond<br>Alkyl | Phe147<br>Met87, Arg333, Phe407, His95, 336, Ile339, Leu406, 415, 416, 417, 420 |
| Seed | XO | XIV | -8.6 | 0.49 | Hydrogen bond<br>Alkyl | Leu257, Lys256, Gly350<br>Ile264, 353 |
| | CytP450 21A2 | XIV | -8.4 | 0.69 | Hydrogen bond<br>Alkyl<br>Attractive charge | Val287, Ser109, Ile291<br>Leu199, Val198, 470, Trp202<br>Asp107, 288 |
| | MPO | XIV | -7.3 | 4.40 | Hydrogen bond | Phe99, Thr100, Arg239, 333 |

be attributed to the polar nature of the tested medium as AA exhibits higher antioxidant activity in a polar medium (Norma et al., 2019). Furthermore, the dose-dependent increase of the callus and seed might be attributed to compounds with high electron-donating capabilities in *A. nilotica* (Mohamed et al., 2009). Additionally, some of the compounds identified in both the callus and seed were linked to antioxidant properties as stated earlier.

In our study, different free radicals-generating enzymes were docked with compounds identified in *A. nilotica* callus and seed to further evaluate the antioxidant potential of the plant. XO catalyzes the rate-limiting step in purine catabolism by utilizing oxygen as an electron donor in place of NAD (Kelley, 2015). This reaction generates superoxide anion free radicals and ROS which further exacerbates conditions associated with oxidative stress. Furthermore, the enzyme

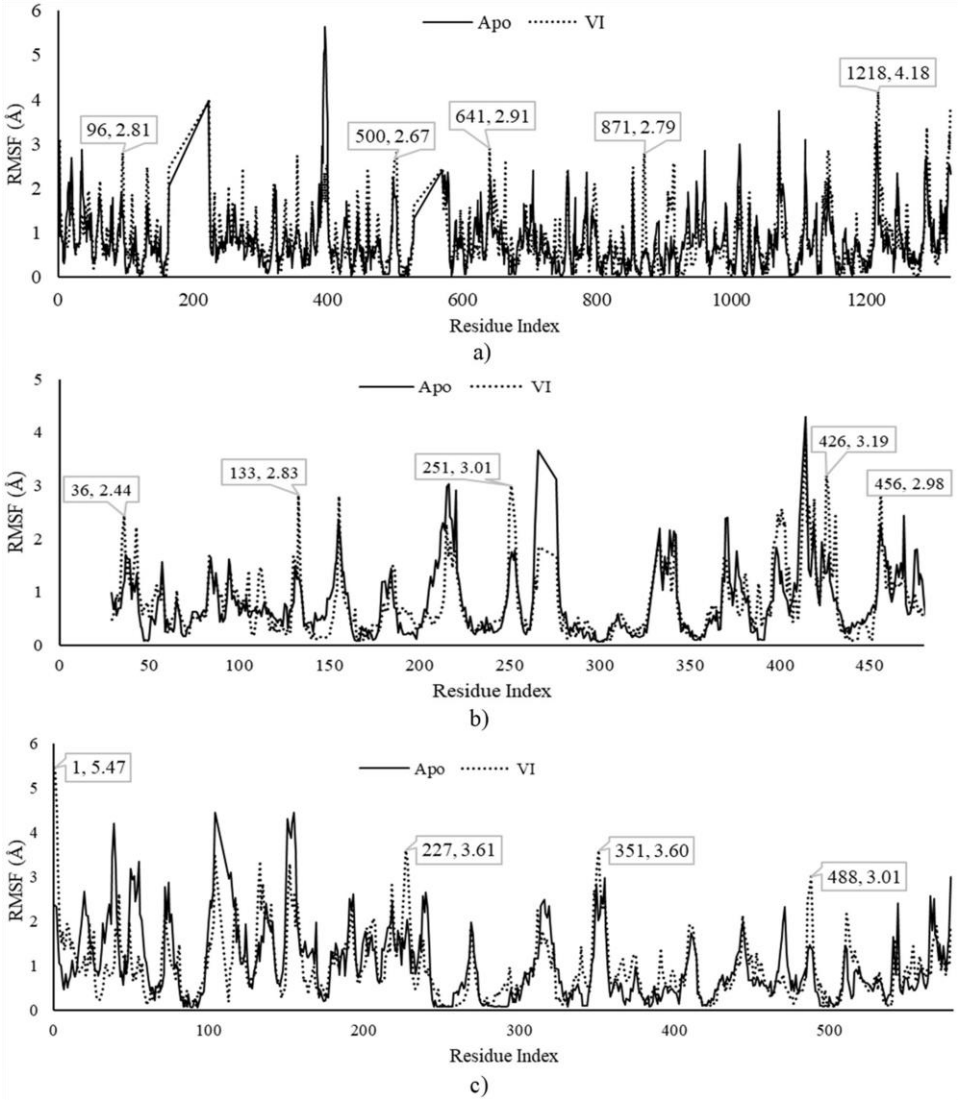


**Figure 7. MDS of Compound VI from the callus docked with; a) XO, b) Cytp450 21A2, and c) MPO. Major increased displacements compared to the apoenzymes are depicted by the data call-outs**

has been linked to free radicals-generating ailments including insulin-resistant diabetes (Hernandez-Hernandez et al., 2022). Hence, this enzyme serves as a therapeutic target to curtail oxidative stress by minimizing its activity. CytP450 21A2 is another enzyme linked to free radicals generation and oxidative stress. It's a monooxygenase enzyme that generates free radicals *via* uncoupled catalytic activity, depicting it as a crucial target for ameliorating oxidative stress in free radicals-generating ailments (Veith & Moorthy, 2018). Another enzyme employed in our study is the MPO which is also linked to free radical generation. MPO is an oxidoreductase secreted by the neutrophils and macrophages as a defense mechanism for the microbicidal effect. This enzyme exerts antimicrobial activity *via* free radical generation from peroxide and chloride to produce HOCl (Chen et al., 2020). Suppression of the enzyme activity might decrease free radical generation and alleviate oxidative stress.

In our study, 22-Stigmasten-3-one (compound VI) identified in the callus exhibited a favorable docking interaction with all the targets, demonstrating the lowest BA and Ki than the other compounds. The BA of the interaction is inversely proportional to the stability of the protein-ligand complex while the Ki expresses the inhibition constant (Kastritis & Bonvin, 2013). The formation of the alkyl interactions within the docking pockets of the enzyme-docked complexes due to compound IV presence might be attributed to the hydrophobic properties of the compound, thus attracting hydrophobic side chains. For the *A. nilotica* seed, 3-(azepan-1-yl)-1,2-benzothiazole 1,1-dioxide (compound XIV) exhibited the most favorable

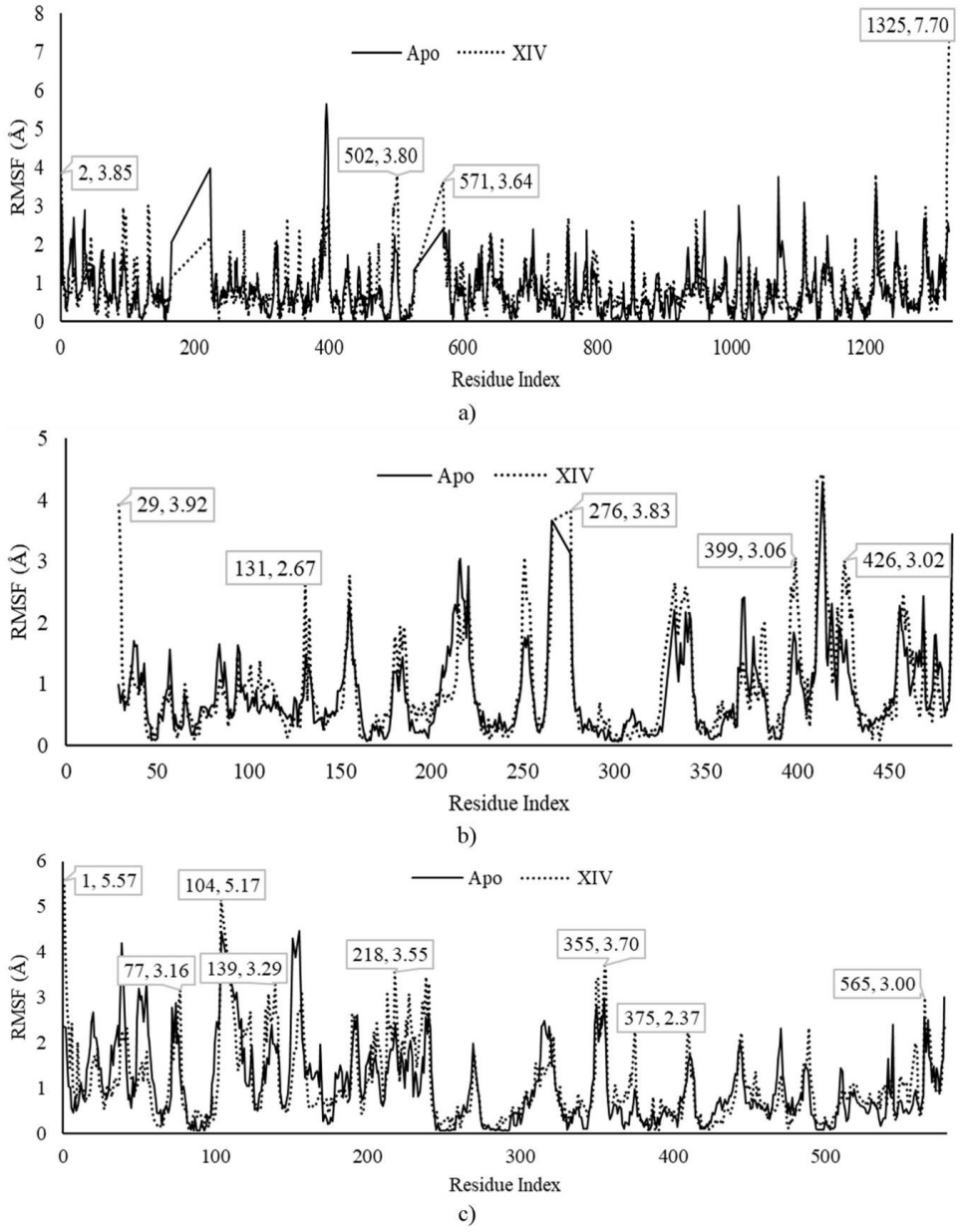


**Figure 8. MDS of Compound XIV from the seed docked with; a) XO, b) Cytp450 21A2, and c) MPO. Major increased displacements compared to the apo-enzymes are depicted by the data call-outs**

docking interactions with the targets, demonstrating the lowest BA and ki than the other compounds. Furthermore, the MDS of the docked complex showed several displaced residues from their mean positions compared to the undocked targets. This might translate to a possible change in conformation and subsequent disruption of enzyme activity. A similar pattern was observed in the MDS for the XIV-docked complex of *A. nilotica* seed. However, the most displaced residues were observed at the N-terminal for XO. Additionally, the callus exhibited higher free radical scavenging activity in both the DPPH and FRAP methods. This correlates with the *in-silico* study as 22-Stigmasten-3-one identified in callus exhibited better interaction with the targets than 3-(azepan-1-yl)-1,2-benzothiazole 1,1-dioxide from the seed.

## CONCLUSION

The present study characterized and explored the antioxidant potential of secondary metabolites obtained the from callus and seed of *A. nilotica*. Conclusively, the callogenesis technique could be a reliable alternative to produce pharmacologically active secondary metabolites and nanoparticles against oxidative stress-linked

ailments. Moreover, 22-Stigmasten-3-one and 3-(azepan-1-yl)-1,2-benzothiazole 1,1-dioxide might be good starting materials for novel therapeutics synthesis against oxidative stress. Additionally, further studies to elucidate their mechanism of action are recommended.

## ACKNOWLEDGEMENT

The authors express their sincere gratitude to the Department of Pharmaceutical Technology of Adamawa State Polytechnic Yola and the Departments of Biochemistry and Biotechnology, Modibbo Adama University Yola for institutional support.

## REFERENCES

AbdelJaleel, G. A., Azab, S. S., el-Bakly, W. M., & Hassan, A. (2021). 'Methyl palmitate attenuates adjuvant induced arthritis in rats by decrease of CD68 synovial macrophages. *Biomedicine and Pharmacotherapy,* 137, 111347. https://doi.org/10.1016/j.biopha.2021.111347

Afrokh, M., Tahrouch, S., Elmehrach, K., Fahmi, F., Bihi, M. A., Weber-Ravn, H., Hatimi, A., & Tabyaoui, M. (2023). Ethnobotanical, phytochemical and antioxidant study of fifty aromatic and medicinal plants. *Chemical Data Collections,* 43, 100984. https://doi.org/10.1016/j.cdc.2022.100984

Ahn, E. Y., & Park, Y. (2020). Anticancer prospects of silver nanoparticles green-synthesized by plant extracts. *Materials Science and Engineering: C,* 116, 111253. https://doi.org/10.1016/j.msec.2020.111253

Arab, H. H., Salama, S. A., Eid, A. H., Kabel, A. M., & Shahin, N. N. (2019). Targeting MAPKs, NF-κB, and PI3K/AKT pathways by methyl palmitate ameliorates ethanol-induced gastric mucosal injury in rats. *Journal of Cellular Physiology,* 234(12), 22424-22438. https://doi.org/10.1002/jcp.28807

Atanasov, A. G., Zotchev, S. B., Dirsch, V. M., & Supuran, C. T. (2021). Natural products in drug discovery: Advances and opportunities. *Nature reviews Drug discovery,* 20(3), 200-216. https://doi.org/10.1038/s41573-020-00114-z

Batiha, G. E.-S., Akhtar, N., Alsayegh, A. A., Abusudah, W. F., Almohmadi, N. H., Shaheen, H. M., Singh, T. G., & De Waard, M. (2022). Bioactive compounds, pharmacological actions, and pharmacokinetics of genus Acacia. *Molecules,* 27(21), 7340. https://doi.org/10.3390/molecules27217340

Benzie, I. F. F., & Strain, J. J. (1996). The ferric reducing ability of plasma (FRAP) as a measure of "antioxidant power": the FRAP assay. *Analytical Biochemistry,* 239(1), 70-76. https://doi.org/10.1006/abio.1996.0292

Chen, S., Chen, H., Du, Q., & Shen, J. (2020). Targeting Myeloperoxidase (MPO) Mediated Oxidative Stress and Inflammation for Reducing Brain Ischemia Injury: Potential Application of Natural Compounds. *Frontiers in Physiology,* 11: 433. https://doi.org/10.3389/fphys.2020.00433

Dahiru, M. M. (2023). Recent advances in the therapeutic potential phytochemicals in managing diabetes. *Journal of Clinical and Basic Research,* 7(1), 13-20. https://jcbr.goums.ac.ir/article-1-385-en.html

Dahiru, M. M., Ahmadi, H., Faruk, M. U., Aminu, H., Hamman, & Abreme, G. C. (2023). Phytochemical Analysis and Antioxidant Potential of Ethylacetate Extract of Tamarindus Indica (Tamarind) Leaves by Frap Assay. *Journal of Fundamental and Applied Pharmaceutical Science,* 3(2), 45-53. https://doi.org/10.18196/jfaps.v3i2.16708

Dahiru, M. M., Alfa, M. B., Abubakar, M. A., & Abdulllahi, A. P. (2024). Assessment of in silico antioxidant, anti-inflammatory, and antidiabetic activites of *Ximenia americana* L. Olacaceae. *Advances in Medical, Pharmaceutical and Dental Research,* 4(1), 1-13. http://dx.doi.org/10.21622/AMPDR.2024.04.1.735

Dahiru, M. M., Badgal, E. B., & Musa, N. (2022). Phytochemistry, GS-MS analysis, and heavy metals composition of aqueous and ethanol stem bark extracts of Ximenia americana. *GSC Biological and Pharmaceutical Sciences,* 21(3), 145-156. http://dx.doi.org/10.30574/gscbps.2022.21.3.0462

Dahiru, M. M., & Musa, N. (2024). Phytochemical Profiling, Antioxidant, Antidiabetic, and ADMET Study of Diospyros mespiliformis Leaf, Hochst Ex A. Dc Ebenaceae. *J. Fac. Pharm. Ankara/Ankara Ecz. Fak. Derg,* 48(2), 412-435. http://dx.doi.org/10.33483/jfpau.1354293

Dahiru, M. M., Musa, N., Abaka, A. M., & Abubakar, M. A. (2023). Potential Antidiabetic

Compounds from Anogeissus leiocarpus: Molecular Docking, Molecular Dynamic Simulation, and ADMET Studies. *Borneo Journal of Pharmacy,* 6(3), 249-277. https://doi.org/10.33084/bjop.v6i3.5027

Dahiru, M. M., & Nadro, M. S. (2022a). Anti-diabetic potential of *Hyphaene thebaica* fruit in streptozotocin-induced diabetic rats. *Journal of Experimental and Molecular Biology,* 23(1), 29-36. https://doi.org/10.47743/jemb-2022-63

Dahiru, M. M., & Nadro, M. S. (2022b). Phytochemical Composition and Antioxidant Potential of Hyphaene thebaica Fruit. *Borneo Journal of Pharmacy,* 5(4), 325-333. https://doi.org/10.33084/bjop.v5i4.3632

Dahiru, M. M., Umar, A. S., Muhammad, M., Fari, I. I., & Musa, Z. Y. (2024). Phytoconstituents, Fourier-Transform Infrared Characterization, and Antioxidant Potential of Ethyl Acetate Extract of Corchorus olitorius (Malvaceae). *Sciences of Phytochemistry,* 3(1), 1-10. https://doi.org/10.58920/sciphy0301208

de Oliveira, M. E. B. S., Sartoratto, A., & Carlos Cardoso, J. (2020). In vitro calli production resulted in different profiles of plant-derived medicinal compounds in Phyllanthus amarus. *Molecules,* 25(24), 5895. https://doi.org/10.3390/molecules25245895

Hamed, A. B., Mantawy, E. M., El-Bakly, W. M., Abdel-Mottaleb, Y., & Azab, S. S. (2020). Putative anti-inflammatory, antioxidant, and anti-apoptotic roles of the natural tissue guardian methyl palmitate against isoproterenol-induced myocardial injury in rats. *Future Journal of Pharmaceutical Sciences,* 6(1), 1-14. https://doi.org/10.1186/s43094-020-00044-y

Hasnain, A., Naqvi, S. A. H., Ayesha, S. I., Khalid, F., Ellahi, M., Iqbal, S., Hassan, M. Z., Abbas, A., Adamski, R., Markowska, D., Baazeem, A., Mustafa, G., Moustafa, M., Hasan, M. E., & Abdelhamid, M. M. A. (2022). Plants in vitro propagation with its applications in food, pharmaceuticals and cosmetic industries; current scenario and future approaches. *Frontiers in Plant Science,* 13(1009395). Retrieved from https://www.frontiersin.org/articles/10.3389/fpls.2022.1009395

Hernandez-Hernandez, M. E., Torres-Rasgado, E., Pulido-Perez, P., Nicolás-Toledo, L., Martínez-Gómez, M., Rodríguez-Antolín, J., Pérez-Fuentes, R., & Romero, J. R. (2022). Disordered Glucose Levels Are Associated with Xanthine Oxidase Activity in Overweight Type 2 Diabetic Women. *International Journal of Molecular Sciences,* 23(19), 11177. https://doi.org/10.3390/ijms231911177

Ishaku, G. A., Haruna, A., Kalum, A. A., Vargas-De-La-Cruz, C., & Solórzano-Acosta, R. (2020). Callogenesis and Antibacterial Activity of Balanites aegyptiaca. *Journal of Biosciences and Medicines,* 8(10), 157-168. https://doi.org/10.4236/jbm.2020.810014

Jaison, J. P., Balasubramanian, B., Gangwar, J., James, N., Pappuswamy, M., Anand, A. V., Al-Dhabi, N. A., Valan Arasu, M., Liu, W.-C., & Sebastian, J. K. (2023). Green Synthesis of Bioinspired Nanoparticles Mediated from Plant Extracts of Asteraceae Family for Potential Biological Applications. *Antibiotics,* 12(3), 543. https://doi.org/10.3390/antibiotics12030543

Jemal, K., Sandeep, B. V., & Pola, S. (2017). Synthesis, characterization, and evaluation of the antibacterial activity of Allophylus serratus leaf and leaf derived callus extracts mediated silver nanoparticles. *Journal of Nanomaterials,* 2017. http://dx.doi.org/10.1155/2017/4213275

Jendele, L., Krivák, R., Škoda, P., Novotný, M., & Hoksza, D. (2019). PrankWeb: a web server for ligand binding site prediction and visualization. *Nucleic Acids Research,* 47, 345-349. https://doi.org/10.1093/nar/gkz424

Kastritis, P. L., & Bonvin, A. M. J. J. (2013). On the binding affinity of macromolecular interactions: daring to ask why proteins interact. *Journal of The Royal Society Interface,* 10(79), 20120835. https://doi.org/10.1098/rsif.2012.0835

Kelley, E. E. (2015). Dispelling dogma and misconceptions regarding the most pharmacologically targetable source of reactive species in inflammatory disease, xanthine oxidoreductase. *Archives of Toxicology,* 89, 1193-1207. https://doi.org/10.1007/s00204-015-1523-8

Khan, M., Hoque, S. M., Hossain, K., Siddique, M., Uddin, K., & Rahman, M. M. (2020). Green Synthesis of Silver Nanoparticles using Ipomoea aquatica Leaf Extract and its Cytotoxicity and Antibacterial Activity Assay. *Green Chemistry Letters and Reviews,*

13. https://doi.org/10.1080/17518253.2020.1839573

Korac, B., Kalezic, A., Pekovic-Vaughan, V., Korac, A., & Jankovic, A. (2021). Redox changes in obesity, metabolic syndrome, and diabetes. *Redox Biology,* 42, 101887. https://doi.org/10.1016/j.redox.2021.101887

Kurcinski, M., Oleniecki, T., Ciemny, M. P., Kuriata, A., Kolinski, A., & Kmiecik, S. (2019). CABS-flex standalone: a simulation environment for fast modeling of protein flexibility. *Bioinformatics,* 35(4), 694-695. https://doi.org/10.1093/bioinformatics/bty685

Lalitha, A., Subbaiya, R., & Ponmurugan, P. (2013). Green synthesis of silver nanoparticles from leaf extract Azhadirachta indica and to study its anti-bacterial and antioxidant property. *International Journal of Current Microbiology & Applied Sciences,* 2(6), 228-235.

Mathur, A., Verma, S. K., Singh, S. K., Prasad, G., & Dua, V. K. (2011). Investigation of the antimicrobial, antioxidant and anti-inflammatory activity of compound isolated from Murraya koenigii. *International Journal of Applied Biology and Pharmaceutical Technology,* 2(1), 470-477.

Mohamad, S. S. N. A., Shameli, K., Teow, S.-Y., Chew, J., Ooi, L.-T., Lee-Kiun Soon, M., Ismail, N. A., & Moeini, H. (2023). Enhanced antibacterial and anticancer activities of plant extract mediated green synthesized zinc oxide-silver nanoparticles. *Frontiers in Microbiology,* 14. https://doi.org/10.1002/jsfa.3532

Mohamed, H., Ons, M., Yosra, E. T., Rayda, S., Neji, G., & Moncef, N. (2009). Chemical composition and antioxidant and radical-scavenging activities of Periploca laevigata root bark extracts. *Journal of the Science of Food and Agriculture,* 89(5), 897-905.

Musa, N., Dahiru, M. M., & Badgal, E. B. (2024). Characterization, In Silico Antimalarial, Antiinflammatory, Antioxidant, and ADMET Assessment of Neonauclea excelsa Merr. *Sciences of Pharmacy,* 3(2), 92-107. https://doi.org/10.58920/sciphar0302232

Namratha, N., & Monica, P. V. (2013). Synthesis of silver nanoparticles using Azadirachta indica (Neem) extract and usage in water purification. *Asian Journal of Pharmacy and Technology,* 3(4), 170-174.

Norma, F. S.-S., Raúl, S.-C., Claudia, V.-C., & Beatriz, H.-C. (2019). Antioxidant Compounds and Their Antioxidant Mechanism. In S. Emad (Ed.), *Antioxidants* (pp. Ch. 2). Rijeka: IntechOpen.

Obidah, A. H., Umaru, A. H., & Shehu, A. S. (2022). Effect of Green Synthesized Iron Oxide Nanoparticles Using Spinach Extract on Triton X-100-Induced Atherosclerosis in Rats. *Biochemistry Research International,* 2022. https://doi.org/10.1155/2022/9311227

Oguntibeju, O. O. (2019). Type 2 diabetes mellitus, oxidative stress and inflammation: examining the links. *International Journal of Physiology, Pathophysiology and Pharmacology,* 11(3), 45–63.

Oh, S., & Kim, D.-Y. (2022). Characterization, Antioxidant Activities, and Functional Properties of Mucilage Extracted from Corchorus olitorius L. *Polymers,* 14(12). https://doi.org/10.3390/polym14122488

Ortiz, C. L. D., Completo, G. C., Nacario, R. C., & Nellas, R. B. (2019). Potential Inhibitors of Galactofuranosyltransferase 2 (GlfT2): Molecular Docking, 3D-QSAR, and In Silico ADMETox Studies. *Scientific Reports,* 9(1), 17096. https://doi.org/10.1038/s41598-019-52764-8

Rahuman, H. H. B., Dhandapani, R., Narayanan, S., Palanivel, V., Paramasivam, R., Subbarayalu, R., Thangavelu, S., & Muthupandian, S. (2022). Medicinal plants mediated the green synthesis of silver nanoparticles and their biomedical applications. *IET nanobiotechnology,* 16(4), 115-144. https://doi.org/10.1049/nbt2.12078

Roy, K. (2013). 'Green'Synthesis of Silver Nanoparticles by using Grape (Vitis Vinifera) Fruit Extract: Characterization of the Particles & Study of Antibacterial Activity. *Research Journal of Pharmaceutical, Biological and Chemical Sciences,* 4(1), 1271-1278.

Sanner, M. F. (1999). Python: a programming language for software integration and development. *Journal of Molecular Graphics and Modelling,* 17(1), 57-61.

Sen, M. K., Nasrin, S., Rahman, S., & Jamal, A. H. M. (2014). In vitro callus induction and plantlet regeneration of Achyranthes aspera L., a high value medicinal plant. *Asian Pacific journal of tropical biomedicine,* 4(1), 40-46. https://doi.org/10.1016/s2221-1691(14)60206-9

Sharma, H. (2017). Role of growth regulators in micropropagation of woody plants-a

review. *International Journal of Advanced Research,* 5(2), 2378-2385. http://dx.doi.org/10.21474/IJAR01/3421

Singh, A., Singh, K., Sharma, A., Kaur, K., Chadha, R., & Singh Bedi, P. M. (2023). Past, Present and Future of Xanthine Oxidase Inhibitors: Design Strategies, Structural and Pharmacological Insights, Patents and Clinical Trials. *RSC Medicinal Chemistry*. https://doi.org/10.1039/D3MD00316G

Sumazian, Y., Syahida, A., Hakiman, M., & Maziah, M. (2010). Antioxidant activities, flavonoids, ascorbic acid and phenolic contents of Malaysian vegetables. *Journal of Medicinal Plants Research,* 4(10), 881-890.

Veerasamy, R., Xin, T. Z., Gunasagaran, S., Xiang, T. F. W., Yang, E. F. C., Jeyakumar, N., & Dhanaraj, S. A. (2011). Biosynthesis of silver nanoparticles using mangosteen leaf extract and evaluation of their antimicrobial activities. *Journal of saudi chemical society,* 15(2), 113-120. https://doi.org/10.1016/j.jscs.2010.06.004

Veith, A., & Moorthy, B. (2018). Role of cytochrome P450s in the generation and metabolism of reactive oxygen species. *Current Opinion in Toxicology,* 7, 44-51. https://doi.org/10.1016/j.cotox.2017.10.003

Zubair, M., Azeem, M., Mumtaz, R., Younas, M., Adrees, M., Zubair, E., Khalid, A., Hafeez, F., Rizwan, M., & Ali, S. (2022). Green synthesis and characterization of silver nanoparticles from Acacia nilotica and their anticancer, antidiabetic and antioxidant efficacy. *Environmental Pollution,* 304, 119249. https://doi.org/10.1016/j.envpol.2022.119249